Nonlinear Performance of Few-Mode Fiber Links with Intermediate Coupling

Filipe M. Ferreira, *Member, IEEE*, Christian S. Costa, Stylianos Sygletos, Andrew D. Ellis

Abstract—this paper reviews and extends the study of nonlinear performance of few-mode fiber links operating in all different linear coupling regimes for different mode delay maps. The single-mode split-step Fourier method is modified to include semi-analytical solutions for linear mode coupling of arbitrary strength. The optimum link configurations minimizing the nonlinear penalty at practical levels of equalization complexity are presented, namely: the coupling strength required to give suppression of nonlinear distortion below the isolated propagation without mode coupling, for different mode delay maps. Finally, the limits of the extension of the single-mode Manakov approximation to the multi-mode case are accurately validated against a fully stochastic model developed considering distribution linear mode coupling.

Index Terms— Mode-division multiplexing, multimode fiber, few-mode fiber, linear mode coupling.

I. INTRODUCTION

MODE-DIVISION MULTIPLEXING (MDM) over few-mode fibers (FMFs) is emerging as an attractive solution to overcome the capacity limit of single-mode fibers (SMFs) [1, 2]. However, the multitude of guided modes introduces new impairments that have to be addressed in order to reach FMFs' full capacity, namely: group delay (GD) spread [3-6] given the interplay between differential mode delay (DMD) and linear mode coupling (XT), and inter-mode nonlinear effects [7-10].

In the linear regime, MDM systems reach is usually limited by the overall GD spread due to XT and DMD, given a maximum equalizer complexity [11, 12]. Even so, ultra-long haul transmission distances can be achieved by using intricate mode delay compensation maps with weak-to-intermediate XT (e.g. 3500 km [13] with six polarization modes), however hard to scale with the number of modes. Conversely, it has been shown that moderate-to-high DMD can be tolerated in the presence of strong XT without the need of compensation maps, above -10dB/km [6, 14].

In the nonlinear regime, it has been shown that MDM systems performance can be dominated by inter-mode interactions for low DMD and low XT [15], and that high XT significantly reduces intermodal nonlinear [16]. However, in the intermediate coupling regime, the nature of the dependence of the nonlinear distortion on the (distributed) XT strength and DMD has only recently started being studied [10, 17] for mode delay uncompensated and compensated links. A significant number of works assume systems operating in the strong mode coupling regime, e.g. [18, 19], and consider a multi-section model where mode coupling is introduced through random unitary matrices each section, where each section must be longer than the linear correlation length. However, mode coupling between groups of non-degenerate modes in FMFs [20-25] are usually of weak or intermediate strength for transmission distances of 100-1000 km. In this way, these models do not cover many of the cases of interest as nonlinear simulations require a step-size much smaller than fibers' nonlinear effective length (~20 km) [26], thus the generation of coupling matrices with the appropriate level of coupling strength for 10-100m is required.

To model nonlinear systems operating in the weak and intermediate linear coupling regime, the introduction of coupling in the form of misaligned fiber splices in each section of a multi-section model was proposed [27]. In this case, the mode coupling matrices are obtained using an overlap integral approach. However, the matrix elements obtained this way are effective in describing the mode power distribution but fail to consider phase effects thereby appropriate only for incoherent sources [28]. Besides, the coupling elements obtained in this way inevitably include mode dependent loss given the nature of the overlap integral not allowing to separately tune the amount of mode coupling and mode dependent loss to be introduced.

Recently, the authors have presented a semi-analytical model capable of describing the linear mode coupling for fibers operating in the intermediate coupling regime [6]. Using such method, the authors matched the analytical predictions for GD in FMF links and validate the GD spreading predictions for different coupling regimes and different link configurations. Furthermore, using such model, the authors were able to accurately study for the first time the nonlinear distortion in FMFs operating in the intermediate coupling regime [10, 17].

In this paper, we review and extend the study of nonlinear

performance of FMFs operating in all different linear coupling regimes for different mode delay maps, in order to find the optimum link configuration minimizing the nonlinear penalty for practical equalization complexities. Section II presents the multi-mode nonlinear model and modifies the split-step Fourier method to include the semi-analytical solution method of the linear mode coupling equations derived in [6]. Section III studies on the impact of linear mode coupling on the inter-mode nonlinear noise for mode delay uncompensated spans, finding the coupling strength required give suppression of nonlinear distortion below the isolated mode without mode coupling. Section IV focus on mode delay compensated links, analyzing the impact of linear mode coupling on the inter-mode nonlinear noise while varying the number of compensation stages. Section V estimates the limits of the regimes under the extension of the single-mode Manakov approximation to the multi-mode case [8, 16] is valid, considering the transmission of wavelength multiplexed channels in each of the polarization modes over the fully stochastic model presented including distributed XT. Conclusions are drawn in Section VI.

II. Nonlinear Propagation Modelling for Extreme and Intermediate Coupling Strength Regimes

The generalized nonlinear Schrödinger equation (GNLSE) for FMFs can be written as [7, 8, 29]:

$$\partial_z A_{ui} + \left(\beta_{ui}^{(1)} \partial_t - \frac{j\beta_{ui}^{(2)}}{2} \partial_t^2 + \ldots + \frac{\alpha_{ui}}{2} \right) A_{ui} = -j\left[\gamma_{uuii} |A_{ui}|^2 \right.$$
$$\left. + 2\gamma_{uvii} \sum_{v\neq u} |A_{vi}|^2 + \frac{2}{3}\gamma_{uvij} \sum_v |A_{vj}|^2 \right] A_{ui} - j\sum_{vk} C_{uvik} A_{vk} e^{j\left(\beta_{ui}^{(0)} - \beta_{vk}^{(0)}\right)z} \tag{1}$$

where i and j are the orthogonal polarizations of mode u. $A_{ui}(z,t)$, $\beta_{ui}^{(1)}$, $\beta_{ui}^{(2)}$ and α_{ui} are the slowly varying field envelope, GD, GD dispersion and attenuation, respectively. γ_{uvij} is the nonlinear coefficient between ui and vj, which depends on the intermodal effective area as shown in [29]. In (1), $\widehat{D}$ is the differential operator that accounts for dispersion and attenuation, and $\widehat{N}$ is the nonlinear operator that accounts for all the intramodal and intermodal nonlinear effects [29]. The last term on the right-hand side accounts for the linear mode coupling arising from fiber structure imperfections, where C_{uvij} are the coupling coefficients as derived in [6].

A. Modified Split-Step Fourier Method

To numerically solve (1), we use a modified version of the split-step Fourier method (SSFM) developed for SMFs. In the SMF case, an approximate solution of the Schrödinger equation is obtained by assuming that over a small distance h the dispersive and nonlinear effects act independently. For FMFs, we extend such an approach by assuming that the mode coupling also acts independently. Such approximation requires h to be much shorter than: the dispersion length $T_0^2/|\beta_u^{(2)}|$, the walk-off length $T_0/|\beta_u^{(1)} - \beta_v^{(1)}|$ (T_0 is the pulse width), and the correlation length L_c defined in [6] such that $XT(L_c) = [e^2 - 1]/[e^2 + 1]$.
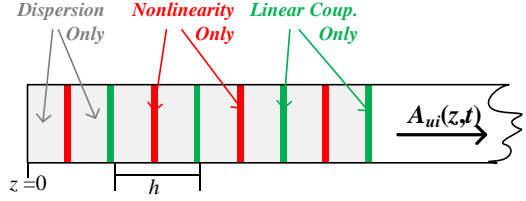

Fig. 1. Schematic illustration of the symmetric SSFM used for numerical simulations.

To include the linear mode coupling, the SSFM is now modified to include an additional step. Fig. 1 presents a schematic illustration of the symmetric SSFM considered for numerical simulations in this paper. By using a symmetric SSFM, the effect of nonlinearity is included in the middle of the segment rather than at the segment boundary providing higher accuracy [30]. Finally, the step-size was selected by bounding the local error [30], more computationally efficient at high accuracy than the other methods, e.g. nonlinear phase rotation.

B. Extreme Coupling Strength Regimes

In the presence of extreme mode coupling strength (weak or strong), it has been shown that the nonlinear distortion can be modelled using averaged coefficients instead of explicitly considering and solving for random coupling matrices. In [7, 8], new Manakov equations were derived for FMFs.

In the weak-coupling (WC) regime [8], it has been found that only the averaging over birefringence fluctuations must be considered, reducing the intramodal degeneracy factor to 8/9 and the intermodal degeneracy factor to 4/3.

$$\widehat{N} = -j\left[\frac{8}{9} \sum_{k=\{i,j\}} \gamma_{uuik} |A_{uk}|^2 + \frac{4}{3} \sum_{\substack{v\neq u \\ k=\{i,j\}}} \gamma_{uvik} |A_{vk}|^2 \right] \tag{2}$$

In the strong coupling (SC) regime [7, 8], the averaging must include all propagation modes. For N-modes, the nonlinear operators for WC and SC are, respectively [7, 8]:

$$\widehat{N} = -j \sum_{\substack{v \\ k=\{i,j\}}} \kappa |A_{vk}|^2, \quad \kappa = \frac{4}{3}\frac{2N}{2N+1}\left(\frac{1}{N^2} \sum_{\substack{u,v \\ k,l=\{i,j\}}} \gamma_{uvkl} \right) \tag{3}$$

C. Intermediate Coupling Strength Regime

In the intermediate coupling regime, (1) must be solved explicitly applying every step new random matrices characteristic of a given coupling strength. In [6], the authors proposed a semi-analytical solution method for the coupled linear differential equations that describe the linear modal coupling in FMFs, this is a solution of (1) assuming the linear mode coupling acting independently as explain in Section II-A, the linear mode coupling step in Fig. 1. The semi-analytical solution method [6] has been proved accurate in the linear power regime. It accurately matched the analytical predictions for the statistics of GDs in FMF links for different transmission lengths 10 m-to-10,000 km, in any coupling regime -50 dB/100m to 0 dB/100m, without and with group delay management. For convenience, the mode coupling strength (XT) is quantified taking the LP01 mode as reference, this is: $XT = \sum_{n\neq LP01} P_n/P_{LP01}$ where P_n is the power of mode n, after a given segment under test, when only mode $LP01$ was launched.

Here, we use the semi-analytical model [6] to implement the linear mode coupling step in Fig. 1. Using this method, the accuracy of full stochastic solutions of (1) will be compared with different analytical expectations, regarding the total nonlinear noise and the nonlinear transmission performance of quadrature amplitude modulated signals.

D. Total Nonlinear Noise: Analytical Integration

The total nonlinear noise generated can be analytically calculated using a generalization of SMFs four-wave mixing (FWM) theory to FMFs [31]. This is, when considering three waves denoted p, q, r propagating in modes denoted a, b, c, respectively, the nonlinear signal A_{ds} generated at angular frequency $\omega_s = \omega_p + \omega_q - \omega_r$ in mode d is:

$$A_{ds} = \xi_{abcd} A_{ap} A_{bq} A_{cr}^* \frac{1 - e^{-\alpha L} e^{-j\Delta\beta_{abcd}L}}{j\Delta\beta_{abcd,pqrs}L + \alpha} \cdot e^{-\alpha/2L} e^{-j\beta_{ds}L} \quad (4)$$

where α is the attenuation and L is the span length. ξ_{abcd} is the total nonlinear coefficient between modes a, b, c, d given by the product of γ_{abcd} and the degeneracy factor dependent on the coupling strength (1)-(3). $\Delta\beta_{abcd,pqrs}$ is the phase mismatch between waves p, q, r, s. The phase mismatch is given by $\Delta\beta_{abcd,pqrs} = \beta_{ap} + \beta_{bq} - \beta_{cr} - \beta_{ds}$ where β_{ap} is the propagation constant of mode a at angular frequency ω_p.

Finally, assuming an optical super-channel with a total bandwidth B the total nonlinear noise between a given set of modes can be calculated by integrating the product of (4) with the signal power spectral density (PSD) in each mode. A closed form solution for this integral was obtained (and experimentally validated) for the case of a signal with a rectangular spectrum (OFDM or Nyquist WDM super channel) in each interacting mode, and the overall efficiency parameter η_{abcd} was shown to be [31]:

$$\eta_{abcd} = \frac{\gamma_{abcd}^2}{\pi\alpha|\beta^{(2)}|} \left[\ln\left(\frac{B^2 + 2B\Delta f_{abcd}}{2f_w} \right) + s \ln\left(s \frac{B^2 - 2B\Delta f_{abcd}}{2f_w} \right) \right], \quad (5)$$

where $\Delta f_{abcd} = (\beta_a^{(1)} + \beta_b^{(1)} - \beta_c^{(1)} - \beta_d^{(1)})/2\pi\beta^{(2)}$, $s = \text{sign}(B - 2\Delta f_{abcd})$, $f_w = \sqrt{\alpha/4\pi^2|\beta^{(2)}|}$, $\beta_a^{(1)}$ is the group delay of mode a, $\beta^{(2)}$ is the second-order dispersion coefficient, and Δf_{abcd} is the velocity-matched frequency offset. In the derivation of (5) it is assumed that [31, 32]: the second-order dispersion coefficient $\beta^{(2)}$ is mode independent; mode group velocities $\beta_a^{(1)}$ are frequency independent; given large $\beta_a^{(0)}$ differences, strong inter-mode phase-matching is only possible for interactions of pairs of modes ($a = d, b = c$ or $b = d, a = c$). According to (5), the FWM efficiency is maximized for frequency offsets Δf_{abcd} at which the walk-off induced by chromatic dispersion and the walk-off induced by mode delay cancel out exactly. Finally, the total nonlinear power generated in mode d is given by $(\sum_{a,b,c} \eta_{abcd}) P_a P_b P_c$, where P_a is the signal power spectral density in mode a.

Fig. 2 shows the nonlinear noise power generated at the center of the WDM signal as a function of the overall bandwidth (B) for a particular six linearly polarized (LP) mode fiber with no linear mode coupling. In addition to the logarithmically increasing background expected for a SMF [33], a number of discontinuities are apparent whenever B becomes sufficiently large to allow strong phase matching
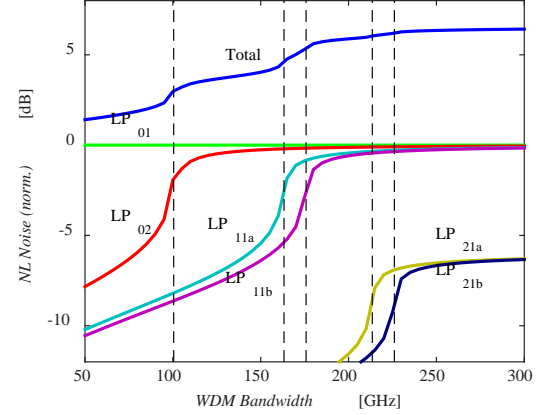

Fig. 2. Contribution to the nonlinear noise power in the LP$_{01}$ mode for signals propagating in higher order modes normalized by the LP$_{01}$ intra-modal nonlinear noise power, as a function of WDM bandwidth.
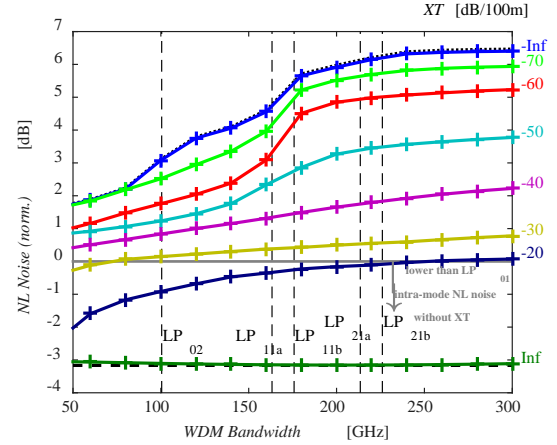

Fig. 3. Total nonlinear noise power in LP$_{01}$ as a function of WDM bandwidth showing analytical predictions from SC (dashed) and WC (dotted) regimes along with numerical simulations (solid) for different XT strengths (colors).

among an additional pair of modes. In Fig. 2, the dashed vertical lines identify these discontinuities ($B/2 = |\Delta f_{abcd}|$). The fiber considered has a graded-index core with a refractive index relative difference of 4.5×10^{-3} and a radius of 12.83 μm, optimized in [34] for low DMD. The fiber characteristics are presented in Table 1. To enhance the visualization of all possible phase matchings, the results in Fig. 2 were obtained with an arbitrary GD vector: (0, 8, 13, 14, 17, 18) ps/km for (LP$_{01}$, LP$_{02}$, LP$_{11a}$, LP$_{11b}$, LP$_{21a}$, LP$_{21b}$), respectively.

III. LINEAR COUPLING IMPACT ON INTERMODAL NONLINEAR NOISE FOR MODE DELAY UNCOMPENSATED SPANS

In this section, the nonlinear noise power is found by solving (1) for a range of different linear coupling strengths ranging from the weak to the strong coupling regimes using the modified SSFM presented in Section II, and by using (5). The simulations assume an optical super-channel with: a rectangular power spectral density (e.g. OFDM), a total WDM bandwidth B, and a subcarrier spacing of 50 MHz (smaller spacing generated similar results). The XT value was varied from -70 to 0 dB/100m covering all coupling values presented in the literature. To the best of our knowledge, the lowest XT values reported are around -50 dB/100m [20] and the highest

XT value reported is -7 dB/100m [35]. Finally, simulations considered the same fiber characteristics as used in Fig. 2.

Fig. 3 shows the nonlinear noise power at the center frequency of the WDM band carried by the LP_{01} mode versus the total WDM bandwidth. The modified SSFM step size was selected by bounding the local error to be lower than 10^{-5} (smaller local errors generated similar results). The simulation results in Fig. 3 lay between two analytical lines obtained with (5) using: the ordinary fiber nonlinear coefficients (for weak mode coupling) [8], dotted line, and using the average nonlinear coefficients derived in [7] for strong mode coupling, dashed line. It can be noted in Fig. 3 that the rate of decrease of the nonlinear noise with *XT* increasing is higher for larger bandwidths than for smaller bandwidths, which shows that the averaging of the nonlinear coefficients among the higher-order modes occurs more rapidly. For small values of *XT*, -70 and -60 dB/100m the steps associated with the inter-mode interactions of LP_{01} with LP_{02} and LP_{21a}/LP_{21b}, become smooth, but the step associated with LP_{11a}/LP_{11b} remains unchanged. This is in line with the asymmetries on the coupling strength between pairs of modes from the same mode groups (stronger) and from different mode groups (weaker) (modes LP_{02} and LP_{21a}/LP_{21b} belong to the same mode group). Increasing *XT* up to -40 dB/100m, smooths the step associated with inter-mode interactions of LP_{01} with LP_{02}. Furthermore, increasing *XT* above -20 dB/100m reduces nonlinear noise power below the LP_{01} intra-mode nonlinear noise power in the absence of linear coupling which was used to normalize the results. In the limit, strongly coupling all modes, using unitary matrices every 10 m (and shorter steps, as verified), the nonlinear noise power matches the analytical results (dashed line) obtained with (5) and the average nonlinear coefficients in [7].

In conclusion, for the crosstalk values shown by the majority of FMFs (from -50 to -20 dB/100m), the nonlinear noise is not accurately estimated by either the weak linear coupling regime or the strong coupling regime. However, the overall conclusion that the stronger coupling reduces nonlinear noise power remains valid. Finally, the reduction of nonlinear noise below that of uncoupled single-mode propagation for linear coupling requires *XT* values above -20dB/100m.

IV. IMPACT OF LINEAR COUPLING ON INTERMODAL NONLINEAR NOISE FOR MODE DELAY COMPENSATED SPANS

To compensate for linear mode coupling and GD spread, multi-input multi-output (MIMO) digital signal processing (DSP) can be used, but DSP complexity increases with the number of modes and the total GD spread. In order to minimize complexity, the total GD spread should typically be reduced to less than 10 ns [36]. DMD managed spans are often used to minimize the GD spread by cascading fibers with opposite sign DMD. A span of length *L* comprised *S* segments, where each segment was itself composed by two fibers of length *L*/*S*/2 with the similar characteristics but opposite sign GD. In the absence of mode coupling, the GD spread at the end of the span would be zero. However, in the presence of coupling, the DMD compensation is no longer fully effective. The impact of the coupling can be minimized by reducing the DMD compensation length to be much smaller than the correlation length set by the coupling [37], however

this might not be practical when correlation length is shorter than typical span distances (50-100 km).
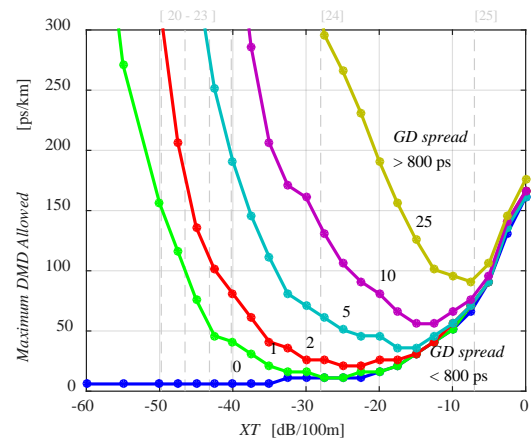

Fig. 4. Contour plot of the pairs (*DMD*, *XT*) that allow for a GD spread lower than 800 ps with a probability higher than 95 %, for 0 to 25 GD compensation segments.
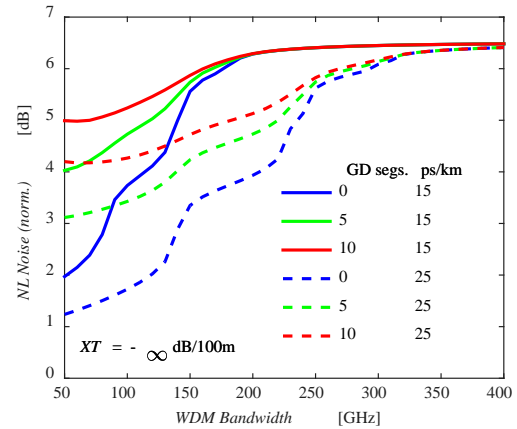

Fig. 5. Total nonlinear noise power in the LP_{01} mode as a function of WDM bandwidth, for [0, 5, 10] compensation segments for *DMD* = [15, 25] ps/km, and *XT* = -∞ dB/100m.

Fig. 4 shows a contour plot of the combinations of (*DMD*, *XT*) that allow for a GD spread lower than 800 ps with a probability higher than 95 %, in the absence of nonlinearities. The GD spread is lower than 800 ps/km for (*DMD*, *XT*) pairs below the curve correspondent to a given numbers of compensation segments. To make analysis straightforward while studying a broad range of DMD scenarios, the results in Fig. 4 were obtained scaling the GD vector in Table I as required after normalization by the highest GD value in the vector, and the segment fibers are assumed to have the exact same characteristics but opposite sign GD. This is, in a segment the first considered is the same used earlier in this paper and optimized in [34] for low DMD, but is not obtained through optimization but just by negating the GD vector, keeping the remaining characteristics of the first fiber. In Fig. 4, for non-GD-managed spans, the maximum tolerable DMD increases with the coupling strength, being very low for weak coupling. For GD-managed spans, as the number of segments increases, increasingly high DMD values are tolerable for weak coupling. For higher levels of coupling (above -30 dB/100m), the tolerable DMD converges to that of the non-GD-managed spans. Importantly, the tolerable DMD

for the GD-managed spans is always ≥ that of non-GD-managed spans.

As mode delay compensation is used and the GD spread is reduced, the total nonlinear noise will increase as phase matching becomes possible for smaller WDM bandwidths. Fig. 5, shows the impact of mode delay compensation on the total nonlinear noise, in the absence of linear mode coupling. We can see that when the WDM bandwidth is small enough such that not all phase matching conditions are meet, the introduction of mode delay compensation increases the total nonlinear noise comparing with the non-compensated case. But if the WDM bandwidth is such that already satisfies all possible phase matchings for non-compensated links, then the introduction of mode delay compensation does not significantly increases the total noise.

From Fig. 4 and Fig. 5 it can be concluded that there is a trade-off between DSP complexity given the GD spread and an increase of the nonlinear noise. To design the optimum FMF link, we will compare the total nonlinear noise falling at the center of the LP_{01} mode, considering the transmission of an optical super-channel with a bandwidth of 1 THz for a given FMF link to that a SMF link, for a broad range of local DMD values and XT values. The nonlinear signal field generated after 100 km was found by following the numerical method presented in Section II. Fig. 5 shows a contour plot of the normalized nonlinear noise power (in dB) generated at the center of the WDM band in the LP_{01} mode, as a function of mode coupling strength and DMD. The nonlinear noise was normalized to the LP_{01} intra-modal nonlinear noise power obtained in the absence of coupling. In Fig. 5, two DMD managed scenarios are shown: (a) 1 segment and (b) 25 segments. Note that, the contour line highlighting the regions from Fig. 4 where the GD spread was higher than 800 ps has been overlapped. In Fig. 5, it can be seen that the nonlinear noise decreases by increasing either the *DMD* value or the *XT* value. Moreover, it can be noted that the nonlinear noise increases with the number of segments, as the contour lines move to higher *DMD* and *XT* values analogously to the enhancement observed for resonant chromatic dispersion managed systems. However, such increase is generally lower than 0.5 dB for the same (*DMD*, *XT*) value as found in [32]. For long period GD maps (Fig. 5-a), the optimum design appears to be to maximize the mode coupling, and operate at the highest possible DMD. However, for shorter period GD-managed maps (Fig. 5-b), for *XT* ranging from -40 to -30 dB/100m since the DMD tolerance increases faster with the number of segments than the nonlinear noise, system performance can be improved by increasing the number of segments and allowing for higher *DMD* values. Importantly, the optimum solution for each GD map (at the highest tolerable DMD for the highest *XT* considered) shows negligible difference in the predicted nonlinear noise.

Fig. 6 shows the nonlinear performance for the highest tolerable DMD (such that GD spread < 800 ps as in Fig. 5) for a broad range of DMD maps. It can be seen that for the XT values given suppression of NL below that of uncoupled propagation (*XT* > -10dB/100m), the usage of DMD

compensation plays no role. Thus, it can be concluded that the usage of high *XT* fibers is preferable given that the deployment complexity associated with GD compensation is removed and fibers with relatively with *DMD* (up to 150 ps/km according to Fig. 6) can still be used.
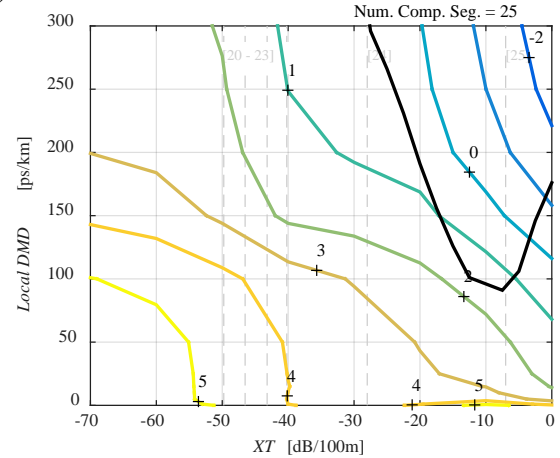
(a)
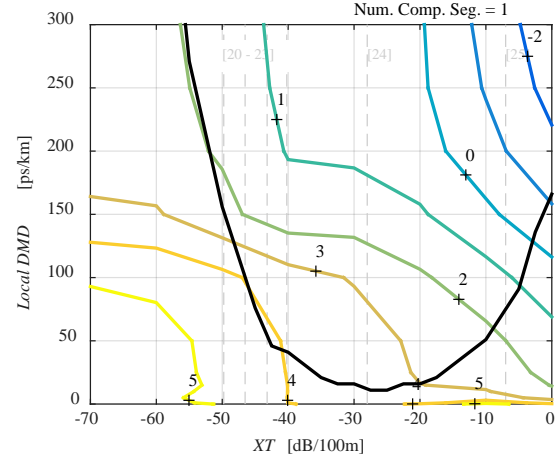
(b)

Fig. 6. Contour plots of the nonlinear noise power in the LP_{01} mode, as a function of mode coupling strength and DMD, normalized by the LP_{01} intra-modal nonlinear noise power (normalized noise values are in dB). Four DMD maps are considered: (1) 1 segment, and (b) 25 segments.
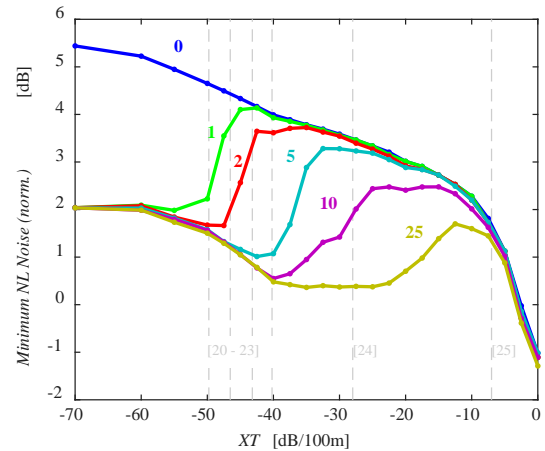

Fig. 7 Minimum nonlinear noise power (normalized) as a function of the mode coupling strength, for a broad range of GD maps ranging from unmanaged to short period.

V. MANAKOV APPROXIMATION VS FULLY STOCHASTIC PROPAGATION

In this section, the link conditions under which the Manakov approximation are accurately established, in terms of uncoupled DMD and linear coupling strength. The validation results in the following consider only mode delay uncompensated links as further results for DMD compensated links generated similar results. The simulations setup and the linear DSP blocks are summarized in the following.

The simulation setup is shown in Fig. 8. Over each polarization mode was transmitted an optical super-channel consisting of 3 channels spaced of 14.1 GHz carrying 14 Gbaud 16-QAM signals, giving a total bit rate of 2 Tb/s (672 Gb/s per wavelength). Together with the information data, a preamble was transmitted consisting of constant amplitude zero autocorrelation (CAZAC) sequences, used for time synchronization and channel estimation. Root raised cosine filters with a roll-off factor of 0.001 were used for pulse shaping. Simulations considered 2^{16} symbols per polarization mode, from which 2^{11} were CAZAC symbols. After homodyne detection, the baseband electrical signals were sampled at 56 GS/s, yielding 12 digital signals at 2 samples/symbol. Afterwards, the coherently received signals were compensated for chromatic dispersion in the frequency domain using the values in Tab. 1. In all cases, mode coupling and (residual) DMD were subsequently compensated for using data-aided channel estimation and equalization, as shown in Fig. 8. Coarse time synchronization was performed using the Schmidl & Cox autocorrelation metric. Subsequently, fine-time synchronization and channel impulse response (CIR) estimation were performed by cross-correlating with the training CAZAC sequences. The 12×12 CIR estimations were converted into the frequency domain. The MIMO frequency domain equalizer was calculated by inverting the channel matrix, and, finally, the *Q-factor* for each received signal was calculated using the mean and standard deviation of the received symbols. In the following, the *Q-factor* was averaged over the 12 polarization modes considering only the centre channels.
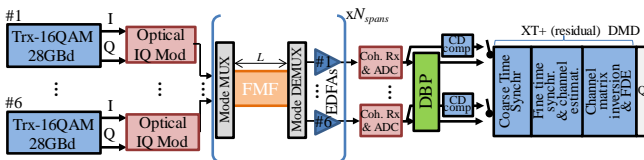
Fig. 8. Block diagram for system simulations using a 6 LP modes.

The fiber attenuation is fully compensated using an array of 6 erbium doped fiber amplifiers [13], considering a noise figure of 3dB and negligible mode dependent gain since the aim of this paper is to assess the isolated impact of mode coupling and mode delay on the Manakov approximation. Moreover, the mode multiplexer (MUX) and de-multiplexer (DEMUX) are assumed ideal for the same reasons.

System performance simulations considered transmission over only 3 spans of 50 km such that at moderate launch signal powers (-5 to 0 dBm) performance was limited by nonlinear noise rather than by spontaneous emission noise, thus enhancing the limitations of the different approximated

nonlinear modelling models. The *DMD* value was varied by scaling the mode group delay values in Tab. 1 to allow for an objective assessment of the Manakov approximation as other fiber characteristics are kept. The *XT* value was varied from -70 to 0 dB/100m (following Section II-C) covering the range of coupling values presented in the literature [20, 24, 35]. The step size was selected by bounding the local error to be lower than 10^{-5}, lower error bounds generated negligible results change.

Simulations included four different methods for the solution of (1), namely: the WC-Manakov approximation (2) [8]; the SC-Manakov (3) [7, 8] approximation; the distributed mode coupling model using the approach presented in Section II-C; a lumped mode coupling model according which random unitary matrices are introduce every L_{lumped} (like in [8]), such that $XT_{[dB/100m]} + 10\log_{10}(L_{lumped}[m]/100[m]) = 0$ dB. To improve the accuracy of the WC- and SC-Manakov models, the uncoupled GD vector was scaled by the ratio between the standard deviation of the coupled GD vector for the *XT* under consideration and the standard deviation of the uncoupled GD vector, using equation (23) in [6] derived through an analytical statistical analysis.
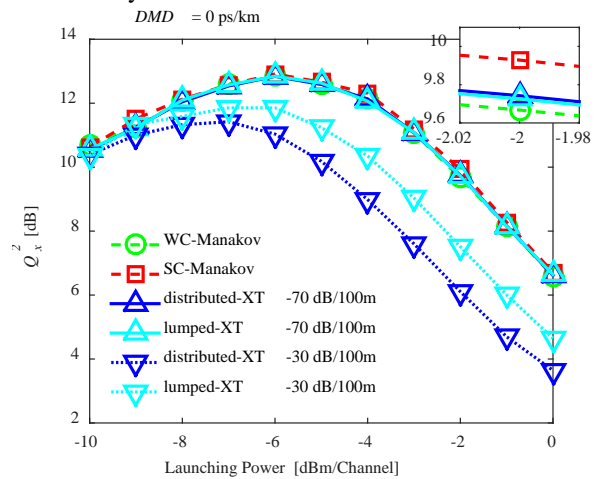
Fig. 9. *Q-factor* as a function of launching signal power in the absence of DMD two different *XT* values: -70 dB/100m (WC-regime), and -30 dB/100m (intermediate coupling regime).

Fig. 9 shows the *Q-factor* as a function of launching power in the absence of DMD for two different *XT* values: -70 dB/100m (WC-regime), and -30 dB/100m (intermediate coupling regime). The figure shows that all models seem to agree for the WC-regime (-70dB/100m), but not so much for the intermediate regime (-30dB/100m). The SC-Manakov and lumped XT models differ by more than 0.5 dB from the distributed XT model in the nonlinear regime. Further insight can be obtained by varying the *XT* and *DMD* while maitaining the a given launching signal power in the nonlinear regime.

Fig. 10 shows the *Q-factor* as a function of *XT* for different models, with -2 dBm/ch, in: (a) the absence of DMD, and (b) the presence of a low *DMD* value, 8 ps/km. First, in all cases Fig. 10-(a) and -(b), WC-Manakov and lumped XT models are in agreement with the distributed XT model for *XT* < -60dB/100m, conversely, SC-Manakov and lumped XT models are in agreement with the distributed XT model for

$XT > $ -10dB/100m. However, in the intermediate coupling regime and for all three DMD cases, the WC- and SC-Manakov models as well as the lumped XT models differ by more than 0.5 dB from the distributed XT model. More importantly, it can be seen that system performance in the nonlinear regime can in fact degrade with increasing XT for low-to-intermediate values (-50 to -30 dB/100m) before it eventually approaches the SC-regime and performance improves above that of the WC-regime, as in Fig. 10-(a) and –(b). Such behaviour can be explained considering that for a certain range of intermediate XT values, additional pathways to FWM phase matching are
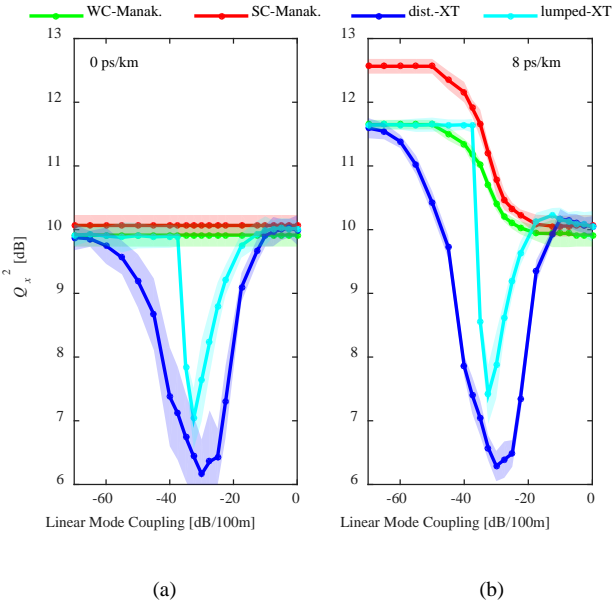

(a)   (b)

Fig. 10. *Q-factor* as a function of mode coupling strength for different channel models/approximations, for -2 dBm/ch and for uncoupled DMD equal to: (a) 0 ps/km, and (b) 8 ps/km. Shadow accounts for 3-times the standard deviation given 20 repetitions.

created without introducing sufficiently fast random rotations of the polarization state of the field along the fiber length which would reduce the efficiency of the overall nonlinear process.

Fig. 10-(b) shows yet another scenario, within the SC-regime, performance degrades with increasing XT. In this case, the performance degradation is due to the severe reduction of the overall GD which allows for phase matching between pairs of modes which were not possible for $XT = -\infty$ dB/100m given the relative narrow bandwidth (42 GHz) of the super-channel considered. Note that the increased penalty is relatively small given that XT reduces GD spread as well as the overall nonlinear coefficients, as explained in Section II-B. Finally, this explantion is in agreement with the behaviour of the SC-Manakov model given the GD vector scaling discussed earlier.

In overall, Fig. 10 shows that to some extent lumped XT model captures the behaviour of the distributed model, even tough overestimating performance by slightly more than 0.5 dB. Finally, Fig. 11 shows *Q-factor error* as a function of mode coupling strength, with the distributed XT model as reference. For extremely small XT values (< -60 dB/100m) WC-Manakov generates accurate results, however pratical fibers have $XT \geq -50$ dB/100m. For high XT values (> -10 dB/100m), SC-

Manakov is only accurate if $DMD < 10$ ps/km, however pratical fibers have higher DMD in particular for more than 3-modes, besides the usage of moderate–to-high DMD fibers in GD-managed links. The lumped XT model is able to accurately model FMF propagation for $XT > -10$ dB/100m even for DMD several times higher than 100ps/km, a pratical scenario, thus an usefull model. Finally, in the intermediate coupling regime (all
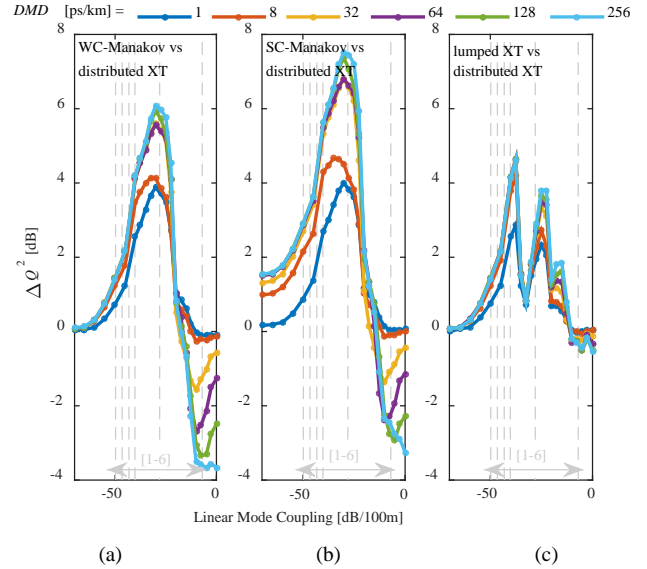

(a)   (b)   (c)

Fig. 11. *Q-factor* error as a function of mode coupling strength, with the distributed XT model as reference, for different models: (a) WC-Manakov model, (b) SC-Manakov model, and (c) lumped XT model. Data points have been averaged over 20 repetitions.

other XT values) only a distributed XT model capable of introducing controlable amounts of XT with a small step-size (1-to-100m) can accurately model tranmission.

VI. CONCLUSIONS

This paper proposes a few-mode split-step Fourier method composed of three steps: dispersion step, nonlinear step, and a linear mode coupling step. The linear mode coupling step is implemented using semi-analytical solutions capable of introducing arbitrary strength coupling in a distributed manner. The proposed model proved accurate against the analytical integration of the total nonlinear noise for optical super-channel with rectangular power spectral densities. Afterwards, the optimum link configurations minimizing the nonlinear penalty at practical levels of equalization complexity were obtained using the proposed model, namely: the coupling strength required to give suppression of nonlinear distortion below the isolated propagation without mode coupling, for different mode delay maps. Furthermore, the proposed model was used to validate the application requirements of models based on Manakov or lumped XT approximations. The proposed model was proved accurate for the extreme regimes not likely in practice (< -50 dB/100m, or > -10 dB/100m with $DMD < 10$ps/km), and the lumped XT model was found to overestimate the system performance by 0.5-to-4 dB in the intermediate coupling regime. Finally, the proposed method is an essential tool for the modelling and development of future high-capacity multimode fiber systems, in particular for the intermediate coupling regime.

APPENDIX

TABLE 1. FIBRE LINEAR CHARACTERISTICS AT 1550NM.

	LP01	LP02	LP11a	LP11b	LP21a	LP21b
GD [ps/km]	0	8.0	13.0	14.0	17.0	18.0
D [ps/(nm.km)]	22.2	21.6	22.2	22.2	21.8	21.8
S [fs/(nm².km)]	66.5	61.5	66.2	66.2	63.7	63.7
α [dB/km]	0.2	0.2	0.2	0.2	0.2	0.2

TABLE 2. NONLINEAR COEFFICIENTS (γ_{uv}) [W^{-1}/KM] AT 1550NM.

u \ v	LP01	LP02	LP11a	LP11b	LP21a	LP21b
LP01	0.72	0.36	0.36	0.36	0.18	0.18
LP02	0.36	0.36	0.18	0.18	0.18	0.18
LP11a	0.36	0.18	0.55	0.55	0.27	0.27
LP11b	0.36	0.18	0.55	0.55	0.27	0.27
LP21a	0.18	0.18	0.27	0.27	0.41	0.41
LP21b	0.18	0.18	0.27	0.27	0.41	0.41

REFERENCES

1. Richardson, D.J., J.M. Fini, and L.E. Nelson, *Space-division multiplexing in optical fibres.* Nature Photonics, 2013. **7**: p. 354.
2. Li, G., et al., *Space-division multiplexing: the next frontier in optical communication.* Advances in Optics and Photonics, 2014. **6**(4): p. 413-487.
3. Marcuse, D., A. Telephone, and T. Company, *Theory of Dielectric Optical Waveguides.* 1991: Academic Press.
4. Ho, K.-P. and J.M. Kahn, *Linear Propagation Effects in Mode-Division Multiplexing Systems.* Journal of Lightwave Technology, 2014. **32**(4): p. 614-628.
5. Antonelli, C., A. Mecozzi, and M. Shtaif, *The delay spread in fibers for SDM transmission: dependence on fiber parameters and perturbations.* Opt Express, 2015. **23**(3): p. 2196-202.
6. Ferreira, F.M., et al., *Semi-Analytical Modelling of Linear Mode Coupling in Few-Mode Fibers.* Journal of Lightwave Technology, 2017. **35**(18): p. 4011-4022.
7. Mecozzi, A., C. Antonelli, and M. Shtaif, *Nonlinear propagation in multi-mode fibers in the strong coupling regime.* Optics Express, 2012. **20**(11): p. 11673-11678.
8. Mumtaz, S., R.-J. Essiambre, and G.P. Agrawal, *Nonlinear Propagation in Multimode and Multicore Fibers: Generalization of the Manakov Equations.* Journal of Lightwave Technology, 2013. **31**(3): p. 398-406.
9. Rademacher, G. and K. Petermann, *Nonlinear Gaussian Noise Model for Multimode Fibers With Space-Division Multiplexing.* Journal of Lightwave Technology, 2016. **34**(9): p. 2280-2287.
10. Ferreira, F.M., et al. *Advantages of strong mode coupling for suppression of nonlinear distortion in few-mode fibers.* in *2016 Optical Fiber Communications Conference and Exhibition (OFC).* 2016.
11. Costa, C.S., et al. *Receiver Memory Requirement in Mode Delay Compensated Few-Mode Fibre Spans with Intermediate Coupling.* in *ECOC 2016; 42nd European Conference on Optical Communication.* 2016.
12. Arik, S.Ö., D. Askarov, and J.M. Kahn, *Effect of Mode Coupling on Signal Processing Complexity in Mode-Division Multiplexing.* Journal of Lightwave Technology, 2013. **31**(3): p. 423-431.
13. Rademacher, G., et al., *Long-Haul Transmission over Few-Mode Fibers with Space-Division Multiplexing.* Journal of Lightwave Technology, 2017. **PP**(99): p. 1-1.
14. Ryf, R., et al. *Long-Distance Transmission over Coupled-Core Multicore Fiber.* in *ECOC 2016 - Post Deadline Paper; 42nd European Conference on Optical Communication.* 2016.
15. Suibhne, N.M., et al. *Experimental verification of four wave mixing efficiency characteristics in a few mode fibre.* in *39th European Conference and Exhibition on Optical Communication (ECOC 2013).* 2013.
16. Antonelli, C., A. Mecozzi, and M. Shtaif. *Scaling of inter-channel nonlinear interference noise and capacity with the number of strongly coupled modes in SDM systems.* in *2016 Optical Fiber Communications Conference and Exhibition (OFC).* 2016.
17. Ferreira, F., et al. *Nonlinear Transmission Performance in Delay-Managed Few-Mode Fiber Links with Intermediate Coupling.* in *Optical Fiber Communication Conference.* 2017. Los Angeles, California: Optical Society of America.
18. Ho, K.-P. and J.M. Kahn, *Statistics of Group Delays in Multimode Fiber With Strong Mode Coupling.* Journal of Lightwave Technology, 2011. **29**(21): p. 3119-3128.
19. Mecozzi, A., C. Antonelli, and M. Shtaif, *Intensity impulse response of SDM links.* Opt Express, 2015. **23**(5): p. 5738-43.
20. Gruner-Nielsen, L., et al., *Few Mode Transmission Fiber With Low DGD, Low Mode Coupling, and Low Loss.* Journal of Lightwave Technology, 2012. **30**(23): p. 3693-3698.
21. An, L., et al. *Reception of mode and polarization multiplexed 107-Gb/s CO-OFDM signal over a two-mode fiber.* in *2011 Optical Fiber Communication Conference and Exposition and the National Fiber Optic Engineers Conference.* 2011.
22. Ryf, R., et al., *Mode-Division Multiplexing Over 96 km of Few-Mode Fiber Using Coherent 6$\times$6 MIMO Processing.* Journal of Lightwave Technology, 2012. **30**(4): p. 521-531.
23. Mori, T., et al. *Low DMD four LP mode transmission fiber for wide-band WDM-MIMO system.* in *2013*

Optical Fiber Communication Conference and Exposition and the National Fiber Optic Engineers Conference (OFC/NFOEC). 2013.

24.   Ryf, R., et al. *Space-Division Multiplexed Transmission over 4200 km 3-Core Microstructured Fiber*. in *National Fiber Optic Engineers Conference*. 2012. Los Angeles, California: Optical Society of America.

25.   Hayashi, T., et al., *Record-Low Spatial Mode Dispersion and Ultra-Low Loss Coupled Multi-Core Fiber for Ultra-Long-Haul Transmission.* Journal of Lightwave Technology, 2017. **35**(3): p. 450-457.

26.   Agrawal, G., *Chapter 2 - Pulse Propagation in Fibers*, in *Nonlinear Fiber Optics (Fifth Edition)*. 2013, Academic Press: Boston. p. 27-56.

27.   Rademacher, G., S. Warm, and K. Petermann, *Influence of Discrete Mode Coupling on the Nonlinear Interaction in Mode-Multiplexed Systems.* IEEE Photonics Technology Letters, 2013. **25**(13): p. 1203-1206.

28.   Shemirani, M.B., et al., *Principal Modes in Graded-Index Multimode Fiber in Presence of Spatial- and Polarization-Mode Coupling.* Journal of Lightwave Technology, 2009. **27**(10): p. 1248-1261.

29.   Ferreira, F., et al., *Nonlinear Semi-Analytical Model for Simulation of Few-Mode Fiber Transmission.* IEEE Photonics Technology Letters, 2012. **24**(4): p. 240-242.

30.   Sinkin, O.V., et al., *Optimization of the split-step fourier method in modeling optical-fiber communications systems.* Journal of Lightwave Technology, 2003. **21**(1): p. 61-68.

31.   Ellis, A.D., et al., *Expressions for the nonlinear transmission performance of multi-mode optical fiber.* Opt Express, 2013. **21**(19): p. 22834-46.

32.   Rademacher, G., S. Warm, and K. Petermann, *Analytical Description of Cross-Modal Nonlinear Interaction in Mode Multiplexed Multimode Fibers.* IEEE Photonics Technology Letters, 2012. **24**(21): p. 1929-1932.

33.   Sinkin, O.V., et al. *Impact of broadband four-wave mixing on system characterization*. in *2013 Optical Fiber Communication Conference and Exposition and the National Fiber Optic Engineers Conference (OFC/NFOEC)*. 2013.

34.   Ferreira, F.M., D. Fonseca, and H.J.A. da Silva, *Design of Few-Mode Fibers With M-modes and Low Differential Mode Delay.* Journal of Lightwave Technology, 2014. **32**(3): p. 353-360.

35.   Fontaine, N.K., et al. *Experimental investigation of crosstalk accumulation in a ring-core fiber*. in *2013 IEEE Photonics Society Summer Topical Meeting Series*. 2013.

36.   Randel, S., et al. *Mode-Multiplexed 6×20-GBd QPSK Transmission over 1200-km DGD-Compensated Few-Mode Fiber*. in *Optical Fiber Communication Conference*. 2012. Los Angeles, California: Optical Society of America.

37.   Arik, S.O., K.-P. Ho, and J.M. Kahn, *Delay Spread Reduction in Mode-Division Multiplexing: Mode Coupling Versus Delay Compensation.* Journal of Lightwave Technology, 2015. **33**(21): p. 4504-4512.